

# Quantifying stabilizing additive hydrolysis and kinetics through principal component analysis of infrared spectra of cross-linked polyethylene pipe

Michael Grossutti, Melanie Hiles, Joseph D'Amico, W. Callum Wareham, Benjamin Morling, Scott Graham, John R. Dutcher\*

Department of Physics, University of Guelph, Guelph, ON N1G 2W1, Canada

## ARTICLE INFO

### Article history:

Received 10 January 2022

Revised 28 April 2022

Accepted 29 April 2022

Available online 2 May 2022

### Keywords:

Cross-linked polyethylene pipe

Infrared microscopy

Hydrolysis

Principal component analysis

## ABSTRACT

Peroxide crosslinked high-density polyethylene (PEX-a) is increasingly being used to replace traditional metal and concrete pipes in applications such as water, gas, and sewage transport. Stabilizing additives play important roles in enhancing the long-term stability of PEX-a pipes and understanding changes to these additives under in-service conditions is critical to further improvements in pipe lifetimes. We used infrared (IR) microscopy to measure spectra within the central portion of the walls of PEX-a pipe subjected to two different types of ageing: exposure to high temperature (85°C) air and exposure to high temperature (85°C) water. To analyze these data, we used principal component analysis (PCA) to implement an unsupervised multivariate analytical approach. This allowed us to identify distinct ageing pathways for the two types of ageing in the two-dimensional space defined by the first two principal components PC1 and PC2, which together account for 88% of the variance in the data. This representation of the data allowed us to associate each PC with different ageing processes in the pipes: changes in PC1 were due primarily to hydrolysis of stabilizing additive ester linkages, whereas changes in PC2 were due primarily to elevated temperature. The PCA showed that ageing in high temperature water produced spectral changes consistent with those measured for an in-service pipe and that water is the key component driving the changes. The results provide important information for PEX-a pipe ageing and stabilizing additive formulation design.

© 2022 Elsevier Ltd. All rights reserved.

## 1. Introduction

Crosslinking of high-density polyethylene using peroxides (PEX-a) results in favorable properties such as high melting temperature and tensile strength. These physical properties, combined with flexibility, ease of installation and resistance to environmental weathering, make PEX-a pipe attractive for use in both indoor and outdoor domestic and industrial applications. PEX-a pipes are certified to withstand exposure to chlorinated water at elevated temperature and pressure [1] so that they resist oxidative degradation during both manufacturing and in-service use. During the manufacturing process, the polyethylene is exposed to high temperature in the presence of oxygen, which can lead to thermo-oxidative degradation such as chain scission [2–4] that makes the pipe susceptible to premature failure [5,6]. During in-service use, PEX-a pipe can be exposed to factors such as oxygen, chlorine, elevated

temperature, and UV light, which can induce thermo-oxidative and photo-oxidative degradation reactions [2–5,7].

To enhance the long-term stability of PEX-a pipe, manufacturers add stabilizing agents, such as primary antioxidants, secondary antioxidants, UV absorbers or hindered amine light stabilizers (HALS). These compounds act either as H-donors that preferentially react with backbone peroxy radicals, or as free-radical scavengers that terminate the pipe degradation by forming stable radical species. However, stabilizing additives can also undergo degradation reactions that reduce their efficacy, and hydrolysis and photodegradation of ester linkages in the amorphous regions of the pipes can lead to leaching of the additives from the pipes into the surrounding water [4,7–10]. The diffusion of oxygen and stabilizing agents within the amorphous regions of the pipe play a fundamental role in these processes, which makes the degree of crystallinity an important factor in degradation kinetics [6,7,9]. Although PEX pipe lifetimes have been established by rigorous stress testing and in-service follow-up, little attention has been paid to the fate of additives under various environmental conditions. Improving the robustness of additives may provide even longer in-

\* Corresponding author.

E-mail address: [dutcher@uoguelph.ca](mailto:dutcher@uoguelph.ca) (J.R. Dutcher).

service life and enable a broader range of permissible operating parameters.

Infrared (IR) spectroscopy is a powerful tool for the study of polyolefins and PEX-a pipe structure, morphology, and ageing. For transmission IR measurements, the strongly absorbing C-H stretching, bending, and rocking IR absorptions of the polyethylene chains are often saturated depending on sample thickness, but weaker IR absorptions contain information on polyethylene crystallinity, polyethylene chain unsaturations, stabilizing additives, and thermo-oxidative degradation products [10]. The IR spectroscopic analysis of polyolefins has often focused on univariate measures of specific absorption bands to quantify different functional group content, for example, carbonyl or vinyl groups [10–16]. The response of these peak intensities to a perturbation of interest, such as elevated temperature or UV exposure, is often tracked as a function of time, temperature or radial position [38–44]. However, PEX-a pipe spectra can be complex, with different correlations between spectral regions and multiple contributions to functional group absorptions. For example, the carbonyl region can contain overlapping contributions from protective stabilizing additives and compounds resulting from oxidative damage. Because of the convoluted nature of the spectra, the interpretation of univariate descriptors can be challenging and potentially misleading.

In this work we use principal component analysis (PCA) to implement a multivariate analytical approach to studying PEX-a IR spectra. PCA can be used to identify and explain the main contributions to the variance in the spectra while also reducing the dimensionality of the dataset. PCA has been shown to be valuable in analyzing many different types of problems and data structures, including spectroscopic studies, in which hundreds of variables corresponding to a variety of physical and chemical properties can be measured with high resolution and are often correlated [17–26]. Recently, we have shown that PCA of IR spectroscopic data of different formulations of PEX-a pipes can be used to characterize and classify different pipe formulations [10].

In the present study, we performed PCA on a dataset containing IR microscopy spectra of axial slices of virgin pipes and pipes subjected to two different ageing protocols – immersion in either hot air (85°C) or hot water (85°C) for extended periods of time – and tracked changes to their IR absorption signatures in the 1800–1520  $\text{cm}^{-1}$  and 1200–895  $\text{cm}^{-1}$  frequency domains. The 1800–1520  $\text{cm}^{-1}$  region contains IR absorptions from carbonyl groups. In PEX-a pipe, IR absorptions in this spectral region can arise from carbonyl-containing ester groups in commonly used commercial polyolefin stabilizing additives (such as Irganox 1010, Irganox 1076, Tinuvin 622, and Tinuvin 700) and from the products of oxidative damage [4,10,27]. This can lead to complex IR band shape with overlapping contributions from beneficial (stabilizing additives) and detrimental (oxidative damage) molecular species. The 1200–895  $\text{cm}^{-1}$  frequency range lies in what is commonly referred to as the fingerprint region of the IR spectrum. In PEX-a pipe, this region contains IR absorption from polyethylene, including those arising from vinyl unsaturations in the polyethylene chain, as well as contributions from stabilizing additives. The C-O vibrations of stabilizing additive ester groups also absorb in this region [4,10,27].

For in-service potable hot water PEX-a pipes, the inner surface is exposed to chlorinated water at elevated temperature, with testing and certification at 60°C for domestic hot water lines and 82°C for commercial hot water lines [28], while the outer surface is exposed to air. In contrast, our hot air and hot water immersion ageing protocols act at both the inner and outer surface of the PEX-a pipe wall. This allows us to isolate the effect of the presence of hot water from that of hot air on our samples (with no contributions from chlorine or pressure). To avoid contributions from the inner and outer surfaces, we restrict our present analysis to spec-

tra collected from the central portions (25%–75%) of the pipe wall thickness.

PCA of the ageing data allowed us to track trajectories for the two different ageing protocols in the two-dimensional space defined by the two leading PCs, PC1 and PC2, which together accounted for 88% of the spectral variance. We found that the spectral changes induced by ageing in hot water at 85°C closely matched those experienced by a potable hot water pipe that had been in-service for longer times. This suggests that hot water specifically, as opposed to hot air, chlorine, or pressure, was the driving force behind the spectral changes observed in the in-service pipe. In addition, we find that PC1, which accounts for 77% of the spectral variance, primarily describes the hydrolysis of an ester linkage associated with a stabilizing additive. We fit the hot water ageing time dependence of PC1 to a simple sigmoidal/logistic function, which allowed us to characterize the time dependence of the hydrolysis reaction. The results of the present study demonstrate the power of PCA of IR microscopy data to identify and track changes to stabilizing additives in PEX-a pipe during ageing at elevated temperature, providing important information to evaluate the long-term stability of PEX-a pipes.

## 2. Materials and methods

### 2.1. Protocols for sample preparation and ageing at elevated temperature

For the ageing experiments at elevated temperature in both air and water, we used segments of extruded PEX-a pipes (21.9 mm inner diameter, 3.2 mm wall thickness, approximately 6 cm in length). The segments were placed in glass beakers and either exposed to air at 85°C or Milli-Q water (resistivity of 18.2  $\text{M}\Omega\text{ cm}$ ) at 85°C. Samples were aged in their respective conditions for a total of 21 days. We chose the conditions for ageing in high temperature air and water to expose the pipe samples to environmental stresses that are similar to those experienced by the outer and inner surfaces of the pipe wall in in-service use. We monitored the progression of the ageing of the pipes at the following time points: 3, 6, 8, 10, 14 and 21 days. At each time point, the samples were removed from the oven and allowed to cool for a minimum of 20 min under room temperature conditions. The samples used in the FTIR microscopy measurements were prepared by slicing the PEX-a pipe samples perpendicular to the extrusion direction using an American Optical model 820 rotary microtome, resulting in thin ( $\sim 100\ \mu\text{m}$  thick) axial slices, as shown schematically in Fig. 1. To ensure that the measured radial changes to pipe properties were due to ageing of the outer and inner pipe walls, and not the ends of the pipe samples, we used the microtome to remove thick slices from the ends of the pipe samples until the combined thickness of the removed slices was  $\sim 4\ \text{mm}$  ( $>$  pipe wall thickness). The microtome was then used to produce the thin axial slices used in the FTIR microscopy experiments. In addition, we measured and analyzed data from axial slices of PEX-a pipe of the same formulation that was either unused (virgin) or used in-service to transport commercial hot water (hot water temperature of 82°C).

### 2.2. FTIR microscopy

Transmission IR absorption spectra were collected for axial slices using a Thermo/Nicolet Continuum Infrared Microscope equipped with an MCT detector at a resolution of 4  $\text{cm}^{-1}$ . Approximately 30 spectra were collected, in 100  $\mu\text{m}$  increments, across the wall thickness of each axial slice to obtain a radial profile of each sample as shown schematically in Fig. 1. Each spectrum represents the average IR absorption over a  $50 \times 50\ \mu\text{m}$  area (at a

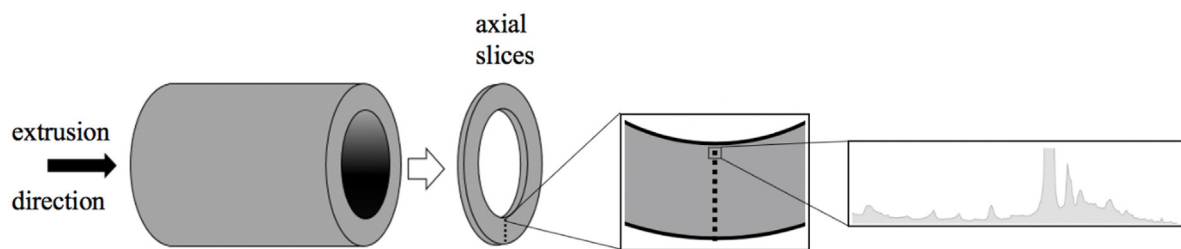


Fig. 1. Sample preparation and experimental geometry used for the FTIR-microscopy experiments performed on axial slices of PEX-a pipe.

given radial depth), expressed in absorbance units:

$$A = -\log(I/I_0) \quad (1)$$

where  $I$  and  $I_0$  are the single beam intensities transmitted through the pipe slice and air respectively.

### 2.3. IR data analysis

Preprocessing of IR spectra was performed in Quasar [29]. Spectra were baseline corrected and normalized by the 2019  $\text{cm}^{-1}$  band, which arises from both amorphous and crystalline regions of polyethylene, to correct for variations in sample thickness [10]. Spectra were mean centered by subtracting the mean spectrum from all spectra in the dataset and principal component analysis (PCA) was performed in Python using the scikit-learn library's `sklearn.decomposition.PCA` [30]. PCA transforms the data into a new feature space of orthogonal PCs defined along the directions of maximum variance in the original data. The PCs are linear combinations of the original features that, in this case, correspond to the detailed dependence of the absorbance on frequency in the IR spectra. Two-dimensional correlation spectroscopy [33,34] was performed using the 2Dpy Jupyter notebook from Shigeaki Morita, Kwansai-Gakuin University [35].

## 3. Results and discussion

We used PCA as an unsupervised learning approach to identify the internal structure of our spectroscopic dataset in a way that best explains the variance in the spectra. In our dataset, the spectral variance was induced in an experimentally controlled fashion through the application of our ageing protocols – immersion in either hot air (85°C) or hot water (85°C) for extended times – to virgin pipes. As the elevated temperature was the same for both protocols, spectral variance induced solely by the increased temperature should be present in the spectra of samples subjected to both protocols. In contrast, spectral variance that depended on the specific ageing medium should result in differences for the two ageing protocols. We note that these ageing protocols mimic, in a limited fashion, the environments experienced by the inner (hot water) and outer (hot air) surfaces of an in-service potable hot water PEX-a pipe. The effects of chlorine and elevated pressure were excluded from the present work to isolate the roles of temperature and the ageing medium. We have also measured spectra from an in-service potable hot water pipe, allowing us to compare the spectral changes induced by our procedures for ageing at elevated temperature to those experienced by the in-service pipe.

In Fig. 2a, we show the results of the PCA of 718 spectra of virgin and aged PEX-a pipe collected from the central portion (25–75% depth) of the pipe wall, where each point represents a single IR spectrum. The PCA model was constructed from the virgin and aged pipe spectra, with the first two PCs accounting for 88% of the spectral variance (PC1 77%, PC2 11%). In Fig. 2a, we also show the PC scores for the in-service potable hot water pipe that were calculated from this model.

In Fig. 2b and c, we show the loading vectors of PC1 and PC2. These loading vectors describe the correlated spectral variance that underpins each PC and can be interpreted as spectra [25,26]. Within each PC loading spectrum, peaks pointing in the same direction are positively correlated whereas peaks pointing in opposite directions are negatively correlated. The physical significance of the PCs can be understood by examining the PC scores in conjunction with the underlying loading spectra.

In Fig. 2a, we show the hot air aged (red), hot water aged (blue) and virgin (gray) PC scores, together with the projected PC scores for the in-service pipe. For a given ageing condition (ageing type and time), the PC scores were clustered together, indicating their close similarity. As the ageing time was increased, the PC scores for the hot air and hot water aged pipes migrated in PC1-PC2 space away from the virgin PC scores, forming distinct ageing trajectories for the hot air and hot water aged pipes. The hot water aged data primarily migrated away from the virgin data along the PC1 axis from negative to positive PC1 values with increased ageing time, with the separation between ageing clusters decreasing as the ageing time increased. In contrast, the hot air aged data primarily migrated along the PC2 axis with increased ageing time, with the separation between ageing clusters much less than in the hot water case, reaching an apparent plateau with substantial overlap of the data for ageing times greater than 8 days. Finally, we can see in Fig. 2a that the projected in-service pipe PC scores coincided closely with those for the 14- and 21-day hot water aged samples, showing that the spectral variance captured by PC1 and PC2 was very similar for these samples.

The physical significance of the hot water ageing trajectory can be understood by examining the PC1 loading spectrum, which is dominated by negative peaks in the carbonyl region between 1800 and 1680  $\text{cm}^{-1}$  (Fig. 2b) and in the fingerprint region between 1180 and 1130  $\text{cm}^{-1}$  (Fig. 2c). The negative loading values indicate that the IR absorbance in these regions was decreasing as the PC1 scores increased from negative to positive values (left to right in Fig. 2a). The negative carbonyl peak is centered at 1737  $\text{cm}^{-1}$  and the negative 1180–1130  $\text{cm}^{-1}$  feature has a minimum at 1160  $\text{cm}^{-1}$  and a shoulder at 1175  $\text{cm}^{-1}$ . The IR spectra of common ester-containing stabilizing additives exhibit strong absorption peaks in these frequency domains [4,10,27], and these frequencies are consistent with carbonyl and C-O absorptions of ester functional groups [31]. Therefore, we attribute the changes captured by PC1 to the loss of ester moieties associated with a stabilizing additive. Furthermore, we note that the extended migration of the PC scores along PC1 occurred only for the hot water aged samples. In contrast, the hot air aged samples experienced a small initial increase in PC1 and then the value of PC1 remained essentially constant for longer ageing times. This behaviour suggests that water is the key component driving the observed spectral changes. Therefore, we propose that the loss of additive-associated ester absorbance was largely due to the water-facilitated hydrolysis of stabilizing additive ester linkages.

The susceptibility of stabilizing additive ester linkages to hydrolysis is well established [9,45–50] and yields a carboxylic

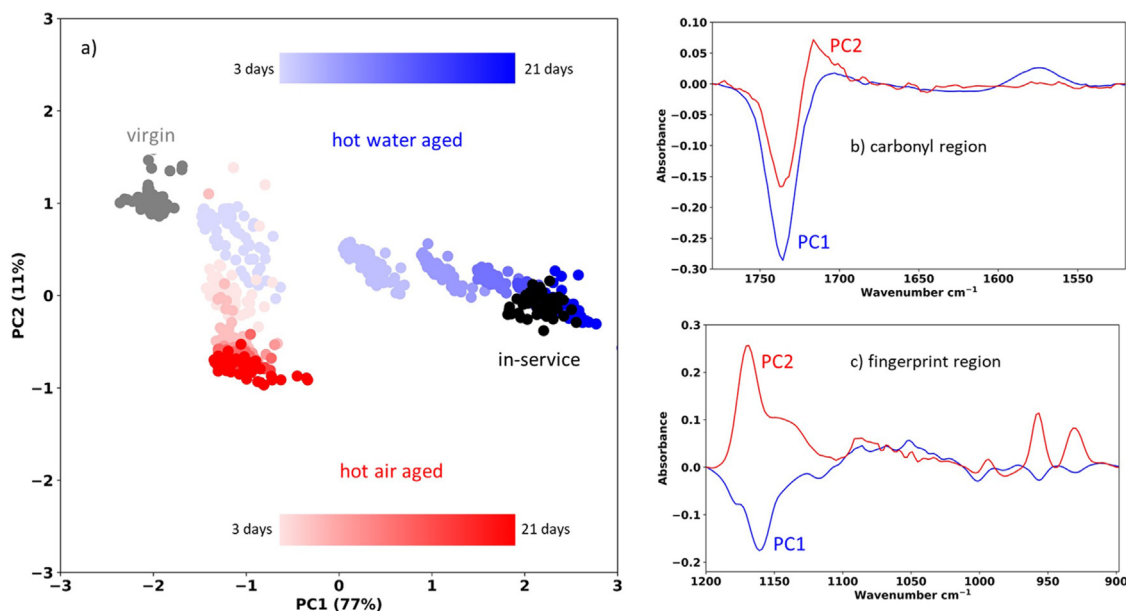


**Fig. 2.** (a) PC score plot for the first two components accounting for 88% of the spectral variance. The PCA model is constructed from virgin (gray), hot air aged (red), and hot water aged (blue) pipe spectra. The PCA model is then applied to the in-service pipe spectra (black) and the spectra are projected onto the PC score plot. The progression to larger ageing times is represented by increasingly darker colours, as indicated in the legends within the plot. (b) Carbonyl region loading spectra for PC1 and PC2. (c) Fingerprint region loading spectra for PC1 and PC2.

acid functional group. Deprotonation of a carboxylic acid COOH yields a carboxylate COO<sup>-</sup> functional group. This deprotonation causes a very large shift in the associated absorbance band from  $\sim 1700\text{ cm}^{-1}$  (COOH) to  $\sim 1570\text{ cm}^{-1}$  (COO<sup>-</sup>). The protonation state of the carboxylic group will be defined by its pKa (at pH = pKa, the group will be 50% deprotonated). We can roughly estimate the pKa of the COOH hydrolysis product to be  $\sim 4.75$  (the pKa acetic acid) [51]. We note that the small positive band at  $1570\text{ cm}^{-1}$  in the PC1 loading spectrum is consistent with an absorption from a carboxylate COO<sup>-</sup> functional group. However, we did not observe any significant absorbance from a COOH functional group. This may be because the pH environment within the pipe wall is sufficiently greater than  $\sim 4.75$  such that the deprotonated COO<sup>-</sup> form is dominant or because the COOH group undergoes further reaction (as discussed below). Furthermore, because the carboxylate peak remained relatively weak during the ageing process, it is likely that there was rapid diffusive loss of small fragments of the hydrolyzed additive to the surrounding water.

The hot air aged trajectory occurred primarily along the PC2 axis, with a small initial jump in the PC1 direction. The PC2 loading spectrum shows a small negative (carbonyl) feature above  $1725\text{ cm}^{-1}$  and a small positive feature below  $1725\text{ cm}^{-1}$ . In the fingerprint region, we observed prominent positive bands at  $1170\text{ cm}^{-1}$  (with a shoulder at  $1145\text{ cm}^{-1}$ ),  $965\text{ cm}^{-1}$ , and  $930\text{ cm}^{-1}$ . The positive peaks indicate that the IR absorbance in these frequency domains was decreasing as the hot air aged PC scores migrated down the PC2 axis to more negative values. A similar decrease in PC2 with ageing time was exhibited by the hot water aged samples. While interpretation of the IR fingerprint region is difficult, we suggest that the changes captured by PC2 were primarily the result of the elevated temperature, as it is the commonality between the air and water aged samples. The physical origin of the IR absorptions described by the PC2 loading spectrum may result from changes to a stabilizing additive or from the loss of trace volatile or reactive compounds after exposure to elevated temperature.

To provide further insight and understanding, we grouped the data points in Fig. 2a into ageing clusters defined by their ageing

conditions (ageing type and time). We calculated the average PC scores for each ageing cluster and show them in Fig. 3a. This averaged representation makes the ageing time dependence of PC1 and PC2 clearer. In Fig. 3b–d we show the averaged spectra for each corresponding ageing cluster, and each point in the PC score plot corresponds to one of the averaged spectra.

The results of the PCA indicate that the averaged hot water and hot air spectra are significantly different. The correlated decrease in IR absorbance in the ester carbonyl and C-O regions in the hot water aged samples is clearly evident in Fig. 3b and c. In contrast, for the hot air aged spectra, little change occurred in the carbonyl region (Fig. 3d) and only an initial decrease was observed in the  $1180\text{--}1130\text{ cm}^{-1}$  region (Fig. 3e). These differences in the averaged hot water aged and hot air aged spectra are essentially the correlated changes that are captured by PC1 and are clearly related to the presence of hot water. Similarly, immediate decreases (and small subsequent decreases) in the  $1180\text{--}1130$ ,  $965$ ,  $930\text{ cm}^{-1}$  regions are evident in both the hot water aged (Fig. 3c) and the hot air aged (Fig. 3e) spectra. In essence, these decreases are the correlated changes that are captured by PC2. Finally, the averaged in-service pipe spectrum corresponds closely with the 14- and 21-days hot water aged spectra in Fig. 3b–c, but differs significantly from all hot air aged spectra in Fig. 3d–e.

We note that oxidation of the pipe samples would produce a significant increase in the carbonyl peak absorbance, which we did not observe. In hot air, there was only a small increase in the carbonyl absorbance (Fig. 3d); and in hot water, we observed large decreases in the carbonyl absorbance (Fig. 3b). These results show that oxidation was not significant when the pipe was exposed to our two ageing protocols within the time scale of the ageing experiments.

We further examine the spectral changes induced by hot water ageing by performing two-dimensional correlation spectroscopy (2DCOS) on the ageing time averaged hot water spectra from Fig. 3b and c. Fig. 4 shows the synchronous correlation spectrum, which describes the simultaneous or coincidental changes in the spectra with ageing time [33,34]. The autopeaks that lie on the diagonal of the synchronous spectrum characterize the magnitude of

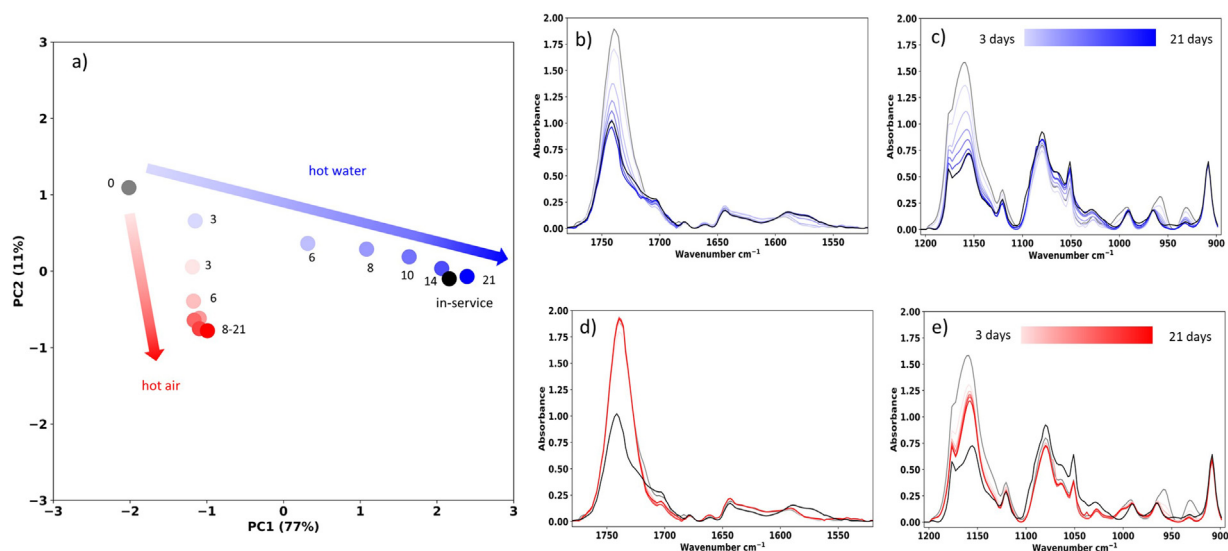


**Fig. 3.** (a) Average PC score plot for virgin (gray), hot air aged (red), and hot water aged (blue) and in-service (black) pipe spectra. The PCA model is constructed from virgin, hot air aged, and hot water aged pipe spectra and applied to the in-service pipe spectra. (b)–(e): Ageing time averaged spectra for the hot water aged samples (carbonyl (b) and fingerprint (c) regions), and hot air aged samples (carbonyl (d) and fingerprint (e) regions). The average virgin (gray) and in-service (black) pipe spectra are also shown in (b)–(e). The progression to larger ageing times is represented by increasingly darker colours, as indicated in the legends within the plots.

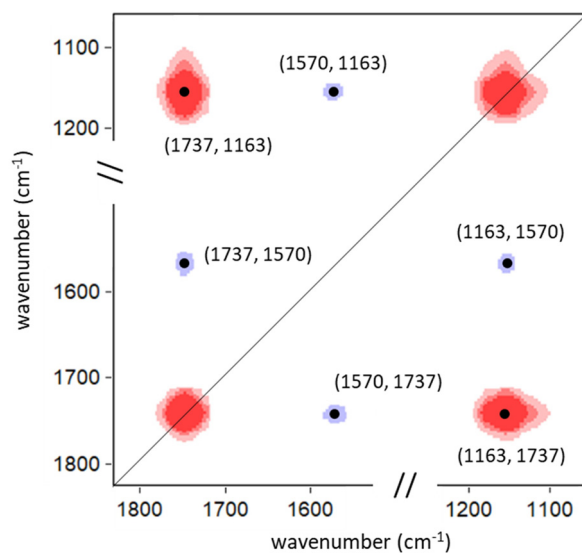


**Fig. 4.** Synchronous 2D correlation spectrum for the hot water aged samples. Red corresponds to positive correlations and blue corresponds to negative correlations. The major cross-peaks and their coordinates are labeled.

the absorbance changes at that frequency [33,34]. The cross-peaks that lie off the diagonal (mirrored on both sides of the diagonal) represent coincidental changes in absorbance at a given frequency coordinate  $(\nu_1, \nu_2)$  [33,34]. A positive cross-peak indicates positive correlation between the coordinate frequencies (and vice versa) [33,34]. The presence of a cross-peak in the synchronous spectrum suggests that a common cause is responsible for the variation in the individual bands [33]. The synchronous spectrum contains strong positive cross-peaks centered at the (1163, 1737) wavenumber coordinates. This means that changes to these spectral regions occur in a simultaneous and coincidental fashion with ageing time. The cross-peak position agreed closely with the major bands in the PC1 loading spectrum. This suggests that the hot water ageing induced changes captured by PC1 occur in coincidental fashion. The synchronous spectrum also contains weaker negative cross-peaks centered at the (1570, 1737) and (1163, 1570) wavenumber coordi-

nates. This means that the carboxylate peak at  $1570\text{ cm}^{-1}$  is negatively correlated with the ester linkage bands and that it grows simultaneously with the decreases in ester absorbance. This is consistent with attributing changes to PC1 with ageing time to ester hydrolysis because the loss of absorbance in the carbonyl and C-O regions and the increase in absorbance of the carboxylate peak must occur simultaneously upon hydrolysis of the ester functional group.

In Fig. 5a and b we show the PC1 and PC2 scores for virgin, hot air aged and hot water aged pipe spectra as a function of ageing time. The corresponding average scores for the in-service pipe are plotted as horizontal black lines. For ageing times of 14–21 days, the PC1 and PC2 scores of the in-service pipe agreed closely with those of the hot water aged pipe. This suggests that hot water ageing closely reproduced changes observed in the central region of the in-service pipe, with respect to phenomena described by PC1 and PC2, which account for 88% of the spectral variance.

PC1 describes the correlated and coincidental changes to the carbonyl and C-O regions that result from the hot water facilitated hydrolysis of stabilizing additive ester linkages. To examine the kinetics of this process we plot PC1 as a function of ageing time in Fig. 6. We also plot the best fit of the PC1( $t$ ) data to a sigmoidal function of the form:

$$a_0 + \left[ \frac{a_1}{1 + e^{(t_0 - t)/\tau}} \right] \quad (2)$$

where  $t$  is the ageing time in days,  $a_0$  is the lower asymptote,  $a_1$  is the difference between the lower and upper asymptotes,  $t_0$  is the center or inflection point of the curve, and  $\tau$  characterizes the width of the curve. S-shaped sigmoidal or logistic functions, such as Eq. (2), are often used to describe the kinetics of second-order autocatalytic reactions such as ester hydrolysis [32].

In Eq. (2), the width of the sigmoidal function is characterized by the time  $\tau$  over which the sigmoidal function increases significantly, e.g., an increase by  $(1/2)(e - 1)/(e + 1) \times 100\% = 23\%$  for  $\Delta t = 2\tau$  about the midpoint of the transition. We extract the best-fit characteristic time constant  $\tau = 2.7$  days from the PC1( $t$ ) data. We note that this timescale, which describes the kinetics of the stabilizing additive ester hydrolysis, is orders of magnitude shorter than the desired service lifetimes of PEX-a pipe. We also note that the S-shaped sigmoidal behaviour exhib-

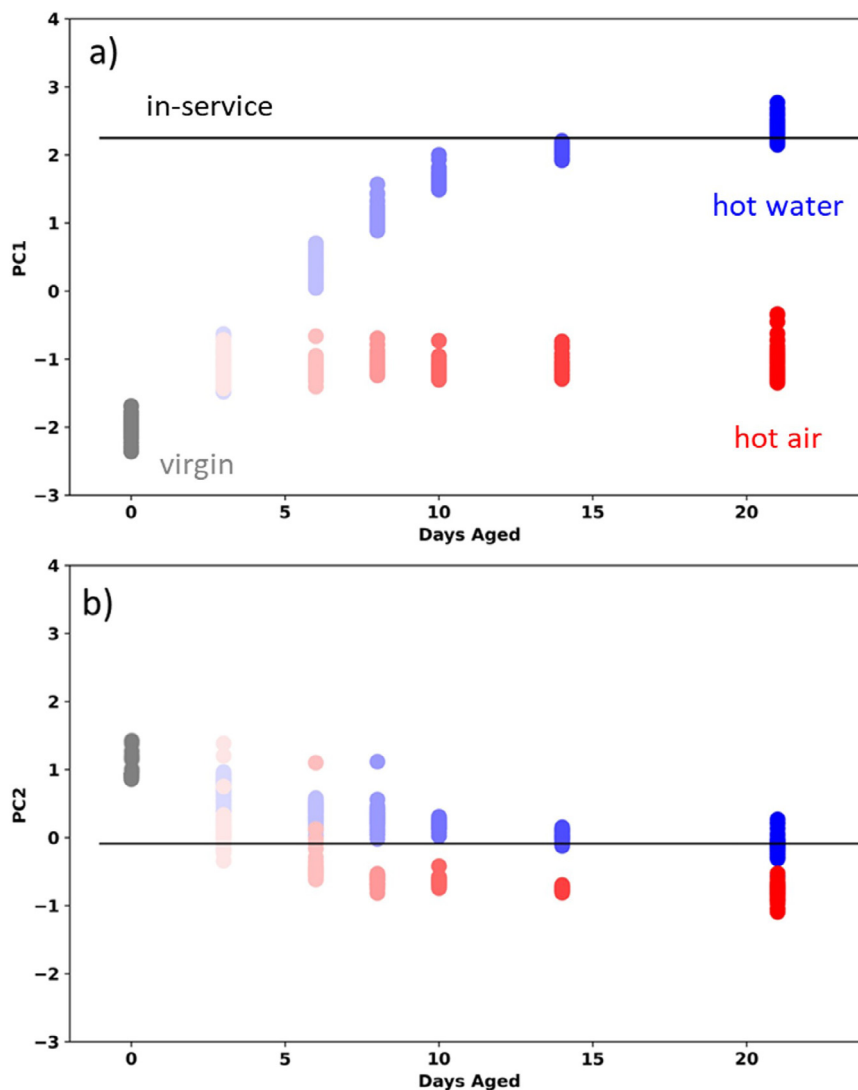


**Fig. 5.** (a) PC1 (77% explained variance) vs days aged, and (b) PC2 (11% explained variance) vs days aged. The progression to larger ageing times is represented by increasingly darker colours. The average scores for the in-service pipe are plotted as horizontal black lines.

ited by  $PC1(t)$  is characteristic of the expected second-order autocatalytic hydrolysis of esters in PEX-a and further supports the attribution of PC1 to stabilizing additive ester hydrolysis. This autocatalytic behaviour may also provide an explanation for the absence of COOH peak in the PC1 additive hydrolysis loading spectrum: the COOH peak may not be observed because it may participate in this autocatalytic hydrolysis. The COOH group and the dissociated hydrogen cation can both act as catalysts for ester hydrolysis [32].

In Fig. 6, we also plot the ageing time dependence of two other features in the IR spectra: the area under the carbonyl peak between 1800 and 1680  $\text{cm}^{-1}$  ( $A_{C=O}$ ), and the area under the 1180–1130  $\text{cm}^{-1}$  feature ( $A_{C-O}$ ). This comparison allows us to interpret the results for the time evolution of the PCA in the context of the specific chemical bonds that characterize the ester functional group. Both  $A_{C=O}(t)$  and  $A_{C-O}(t)$  decrease as ester hydrolysis progresses and they are well described by the sigmoidal function in Eq. (2), which is consistent with the heavy weighting of these peaks in the PC1 loading spectrum (Fig. 2). The best-fit value of  $\tau = 2.2$  days for  $A_{C=O}(t)$  is similar to that of  $PC1(t)$ , which is reasonable since the PC1 loading spectrum has a dominant contribution from  $A_{C=O}$ , and PC2 (which does not describe hydrolysis) has only a minor contribution from  $A_{C=O}$ . In contrast, the best-fit

value of  $\tau = 3.6$  days for  $A_{C-O}(t)$  is significantly larger than that for  $PC1(t)$ . This can be understood by examining the PC1 and PC2 loading spectra.

The PC1 loading spectrum has a strong contribution from  $A_{C-O}$  and so  $A_{C-O}(t)$  retains the sigmoidal character of ester hydrolysis. However, the PC2 loading spectrum also has a major contribution from  $A_{C-O}$ . This overlapping contribution from an uncorrelated process causes a significant change in  $\tau$  for  $A_{C-O}(t)$  compared to that for  $PC1(t)$ . A key advantage of the PCA is the extraction, through PC1, of the correlated spectral variance between the  $A_{C=O}$  and  $A_{C-O}$  frequency domains and its decoupling from overlapping but uncorrelated spectral variance captured by PC2. This enables the characterization of stabilizing additive hydrolysis despite overlapping spectral contributions that would otherwise convolute an analysis of univariate metrics (e.g.,  $A_{C=O}$  and  $A_{C-O}$ ).

In Fig. 6 we also plot the average PC2 scores for hot water and hot air aged pipes as a function of ageing time, as well as the best fit of the  $PC2(t)$  data to an exponential function of the form:

$$a_0 + a_1 e^{-t/\tau} \quad (3)$$

where  $t$  is the ageing time in days,  $a_0$  and  $a_1$  are constants, and  $\tau$  is the characteristic time constant.

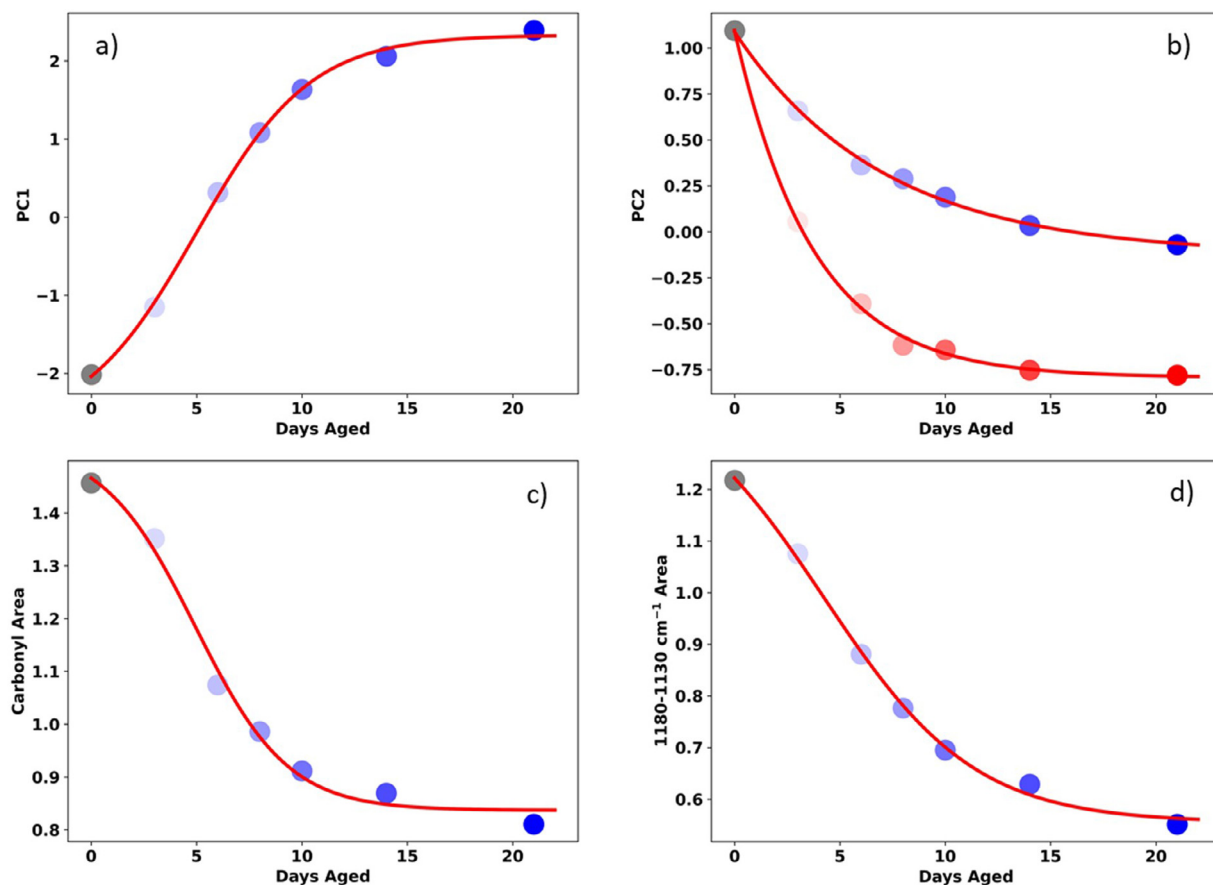


**Fig. 6.** (a) The average hot water aged PC1 scores versus ageing time  $t$  in days. The solid red line was calculated using Eq. (2) and the best-fit ( $r^2 = 0.999$ ) parameter values:  $a_0 = -2.7$ ,  $a_1 = 5.1$ ,  $t_0 = 5.0$  days, and  $\tau = 2.7$  days. (b) The average hot water and hot air aged PC2 scores versus ageing time  $t$  in days. The solid red lines were calculated using Eq. (3) and the best-fit ( $r^2 = 0.998$ ) parameter values for hot air  $a_0 = -0.79$ ,  $a_1 = 1.9$ , and  $\tau = 3.7$  days, and hot water  $a_0 = -0.12$ ,  $a_1 = 1.2$ , and  $\tau = 7.0$  days. (c) The average hot water aged carbonyl area  $A_{C=O}$  versus ageing time  $t$  in days. The solid red line was calculated using Eq. (2) and the best-fit ( $r^2 = 0.992$ ) parameter values:  $a_0 = 0.84$ ,  $a_1 = 0.70$ ,  $t_0 = 4.9$  days, and  $\tau = 2.2$  days. (d) The average hot water aged 1180–1130  $\text{cm}^{-1}$  area  $A_{C-O}$  versus ageing time  $t$  in days. The solid red line was calculated using Eq. (2) and the best-fit ( $r^2 = 0.998$ ) parameter values:  $a_0 = 0.55$ ,  $a_1 = 0.87$ ,  $t_0 = 4.2$  days, and  $\tau = 3.6$  days. For each plot, the progression to larger ageing times is represented by increasingly darker colours.

For both the hot air and hot water aged samples,  $PC2(t)$  is well characterized by a simple first-order exponential function (Eq. (3)). We extract best-fit time constants  $\tau = 3.7$  days for the hot air aged samples and  $\tau = 7.0$  days for the hot water aged samples. We suggest that PC2 primarily captures the relatively small effect of elevated temperature on the spectra, perhaps due to the loss of trace volatile or reactive compounds. The smaller value of  $\tau$  observed for the hot air aged samples compared to the hot water aged sample suggests that oxygen may play a role in these changes.

We can compare the averaged spectra (Fig. 3b and c) that correspond to the plateau at long ageing times in Fig. 6a. We note that the PC1 loading spectrum exhibited a negative carbonyl peak centred at a frequency of  $1737 \text{ cm}^{-1}$ , which is consistent with the carbonyl frequency associated with ester carbonyl groups and common stabilizing additives. Despite the loss of this ester carbonyl associated absorbance that occurred during the hot water ageing protocol, we note that a high frequency carbonyl absorbance at  $1742 \text{ cm}^{-1}$  peak remained prominent in the 14- and 21-day hot water ageing spectra (and in the in-service pipe spectrum). This frequency is also consistent with an ester carbonyl in common stabilizing additives. It may result from a second ester-containing stabilizing additive that has not undergone hydrolytic cleavage of its ester linkage, since multiple stabilizing additives are typically included in commercial pipe formulations. Stabilizing additives with long linear chain structures and sterically accessible ester linkages, such as Tinuvin 622, will be more susceptible to hydrolysis

than those with more compact structures, such as Irganox 1010, which contains sterically sheltered ester linkages. It is possible that we are observing the hydrolysis of one of two different ester-containing stabilizing additives.

Our findings in the present study have important implications for PEX-a pipe formulation design, as the timescale over which we observe significant hydrolysis (days) in our hot water immersion ageing experiments is much shorter than the desired lifetimes of PEX-a pipes (decades). This large discrepancy between the hydrolysis timescale and the desired lifetime indicates that some of the stabilizing additives are short-lived in PEX-a pipe. The use of ester-linked oligomeric stabilizer additives (such as Tinuvin 622) is intended to reduce their migration within the pipe wall and surface volatility [36,37]. Cleavage of this linkage will reduce the molecular weight of the stabilizing additive, which could lead to increased diffusion and decreased performance. It is important that the design of stabilizing additives avoids these unwanted effects.

The hydrolysis and extraction of ester-linkage containing stabilizing additives in polyolefin systems is well established [9,45–50]. These studies often characterize the stabilizing additive and/or hydrolysis products via the analysis of water extractions from the polyolefin [9,45] and/or through organic solvent treatment and extraction protocols applied to the water-treated polyolefin [9,46,47]. The application of PCA to IR spectra of aged PEX-a pipe complements these focused approaches to studying stabilizing additive hydrolysis. But more broadly, this work demonstrates how a

simple unsupervised learning approach like PCA can result in the data-driven discovery of informative features (which in this case corresponds to PC1 describing stabilizing additive hydrolysis) in a dataset of PEX-a pipe IR spectra. This approach is robust, broadly applicable, and is not limited or tailored to stabilizing additive hydrolysis or indeed any specific physicochemical process.

Finally, we note that commercial formulations of PEX-a pipe typically incorporate proprietary additive packages from third party suppliers so that the details of the stabilizing additives are not known by the manufacturers of PEX-a pipe. Despite this lack of precise knowledge of the specific stabilizing additives, in the present study we have identified and quantified spectroscopic changes that occurred during the ageing procedures and, in the case of exposure to hot water, identified the underlying process – the hydrolysis of ester linkages corresponding to changes in PC1. This speaks to the generality of our approach and its applicability to the analysis of ageing of commercial PEX-a pipes.

#### 4. Summary and conclusions

We have evaluated PEX-a pipes subjected to ageing by performing PCA on IR microscopy measurements of the pipes. We found that a large amount (88%) of the spectral variance was described by the two leading principal components, PC1 and PC2. This allowed us to focus on these two PCs and to identify distinctive ageing pathways in PC1 – PC2 space for our two ageing protocols: immersion in hot air and immersion in hot water. By examining the main IR signal contributions to PC1 and PC2, we were able to associate distinctive physical changes with each PC: PC1 (77%) was primarily associated with the hydrolysis of stabilizing additive ester linkages and PC2 (11%) was primarily associated with the elevated temperature. Using the PCA model, we calculated the PC1 and PC2 scores for the spectra of an in-service potable hot water pipe and found that they coincided closely with those immersed in hot water for 14–21 days. This suggests that hot water, as opposed to hot air, chlorine, or pressure, is the key component driving ageing in the central portion of the in-service pipe wall. Furthermore, we found that the PC1 data for pipe aged in hot water at 85°C increased in a sigmoidal fashion with ageing time, with a characteristic time of  $\tau = 2.7$  days, which is consistent with the second-order autocatalytic hydrolysis of ester linkages in a stabilizing additive. Our results have revealed key information with respect to PEX-a pipe ageing and have important implications for the design and selection of stabilizing additives for PEX-a pipe formulations.

#### Funding

This work was supported by the [Natural Sciences and Engineering Research Council of Canada](#) [grant number CRDPJ-2018-531166].

#### Declaration of Competing Interest

The authors declare that they have no known competing financial interests or personal relationships that could have appeared to influence the work reported in this paper.

#### CRedit authorship contribution statement

**Michael Grossutti:** Conceptualization, Methodology, Formal analysis, Visualization, Writing – original draft. **Melanie Hiles:** Investigation, Formal analysis. **Joseph D'Amico:** Investigation. **W. Callum Wareham:** Data curation. **Benjamin Morling:** Investigation. **Scott Graham:** Investigation. **John R. Dutcher:** Conceptualization, Methodology, Funding acquisition, Supervision, Writing – review & editing.

#### Acknowledgments

We thank Jacek Lipkowski and Peter Kazmaier for valuable discussions. J.R.D. is the recipient of a College of Engineering and Physical Sciences Research Chair in Novel Sustainable Nanomaterials.

#### References

- [1] ASTM Standard F2023-15, Standard test method for evaluating the oxidative resistance of crosslinked polyethylene (PEX) pipe, tubing and systems to hot chlorinated water (2015).
- [2] M. Hakkarainen, A.C. Albertsson, Environmental degradation of polyethylene, *Adv. Polym. Sci.* 69 (2004) 177–199.
- [3] T. Ojeda, A. Freitas, K. Birck, E. Dalmolin, R. Jacques, F. Bento, F. Camargo, Degradability of linear polyolefins under natural weathering, *Polym. Degrad. Stab.* 96 (4) (2011) 703–707.
- [4] R. Maria, Monitoring the Degradation of PE Pipes by IR-Microscopy, Ph.D. Thesis, Technical University of Darmstadt (2014).
- [5] S. Al-Malaika, C. Goodwin, S. Issenhuth, D. Burdick, Perspectives in stabilization of polyolefins, *Polym. Degrad. Stab.* 64 (1) (1999) 145.
- [6] L.C. Mendes, E.S. Rufino, F.O. De Paula, A.C. Torres, Mechanical, thermal and microstructure evaluation of HDPE after weathering in Rio de Janeiro City, *Polym. Degrad. Stab.* 79 (2003) 371–383.
- [7] R. Maria, K. Rode, T. Schuster, G. Geertz, F. Malz, A. Sanoria, H. Oehler, R. Brüll, M. Wenzel, K. Engelsing, M. Bastian, E. Brendlé, Ageing study of different types of long-term pressure tested PE pipes by IR-microscopy, *Polymer* 61 (2015) 131–139.
- [8] M. Scoconi, S. Cimmino, M. Kaci, Photo-stabilisation mechanism under natural weathering and accelerated photo-oxidative conditions of LDPE films for agricultural applications, *Polymer* 41 (2000) 7969–7980.
- [9] K. Thörnblom, M. Palmlöf, T. Hjertberg, The extractability of phenolic antioxidants into water and organic solvents from polyethylene pipe materials – Part I, *Polym. Degrad. Stab.* 96 (10) (2011) 1751–1760.
- [10] M. Hiles, M. Grosutti, J.R. Dutcher, Classifying formulations of crosslinked polyethylene pipe by applying machine-learning concepts to infrared spectra, *J. Polym. Sci. Part B Polym. Phys.* 57 (2019) 1255–1262.
- [11] J. Viebke, E. Elble, M. Ifwarson, U.W. Gedde, Degradation of unstabilized medium-density polyethylene pipes in hot-water applications, *Polym. Eng. Sci.* 34 (17) (1994) 1354–1361.
- [12] K. Karlsson, G.D. Smith, U.W. Gedde, Molecular structure, morphology, and antioxidant consumption in medium density polyethylene pipes in hot-water applications, *Polym. Eng. Sci.* 32 (10) (1992) 649–657.
- [13] N.M. Stark, L.M. Matuana, Surface chemistry and mechanical property changes of wood-flour/high-density-polyethylene composites after accelerated weathering, *J. Appl. Polym. Sci.* 94 (6) (2004) 2263–2273.
- [14] L.A. Pinheiro, M.A. Chinelatto, S.V. Canevarolo, The role of chain scission and chain branching in high density polyethylene during thermo-mechanical degradation, *Polym. Degrad. Stab.* 86 (3) (2004) 445–453.
- [15] J. Fu, B.W. Ghali, A.J. Lozynsky, E. Oral, O.K. Muratoglu, Ultra high molecular weight polyethylene with improved plasticity and toughness by high temperature melting, *Polymer* 51 (12) (2010) 2721–2731.
- [16] R. Yang, Y. Liu, J. Yu, K. Wang, Thermal oxidation products and kinetics of polyethylene composites, *Polym. Degrad. Stab.* 91 (8) (2006) 1651–1657.
- [17] A.G. Ryder, Classification of narcotics in solid mixtures using principal component analysis and Raman spectroscopy, *J. Forensic Sci.* 47 (2) (2002) 275–284.
- [18] H.H. Nieuwoudt, B.A. Prior, I.S. Pretorius, M. Manley, F.F. Bauer, Principal component analysis applied to fourier transform infrared spectroscopy for the design of calibration sets for glycerol prediction models in wine and for the detection and classification of outlier samples, *J. Agric. Food Chem.* 52 (2004) 3726.
- [19] E. Kaznowska, J. Depciuch, K. Szmuc, J. Cebulski, Use of FTIR spectroscopy and PCA-LDC analysis to identify cancerous lesions within the human colon, *J. Pharm. Biomed. Anal.* 134 (2017) 259.
- [20] K. Janne, J. Pettersen, N.O. Lindberg, T. Lundstedt, Hierarchical principal component analysis and projection to latent structure technique on spectroscopic data as a data pretreatment for calibration, *J. Chemom.* 15 (2001) 203.
- [21] J. Guicheteau, L. Argue, D. Emge, A. Hyre, M. Jacobson, S. Christesen, Bacillus spore classification via surfaced-enhanced raman spectroscopy and principal component analysis, *Appl. Spectrosc.* 62 (3) (2008) 267.
- [22] G. Bellisola, M.B. Vittori, G. Cinque, P. Dumas, Z. Fiorini, C. Laudanna, M. Mirenda, C. Sandt, G. Silvestri, L. Tomasello, M. Vezzalini, Unsupervised explorative data analysis of normal human leukocytes and BCR/ABL positive leukemic cells mid-infrared spectra, *Analyst* 140 (13) (2015) 4407–4422.
- [23] C. Peng, F. Chiappini, S. Kaščáková, M. Danulot, C. Sandt, D. Samuel, P. Dumas, C. Guettier, F. Le Naour, Vibrational signatures to discriminate liver steatosis grades, *Analyst* 140 (4) (2015) 1107–1118.
- [24] J. Pijanka, G.D. Sockalingum, A. Kohler, Y. Yang, F. Draux, G. Parkes, K.P. Lam, D. Collins, P. Dumas, C. Sandt, D.G. Van Pittius, Synchrotron-based FTIR spectra of stained single cells. Towards a clinical application in pathology, *Lab. Investig.* 90 (5) (2010) 797–807.
- [25] C. Modugno, C. Peltier, H. Simonin, L. Dujourdy, F. Capitani, C. Sandt, J.M. Perrier-Cornet, Understanding the effects of high pressure on bacterial spores using synchrotron infrared spectroscopy, *Front. Microbiol.* 10 (2020) 3122.

- [26] C.B.Y. Cordella, I.S. Krull, in: *Analytical Chemistry*, Croatia, 2012, pp. 1–46. In-Tech.
- [27] Wiley Spectrabase, <https://spectrabase.com/>
- [28] NSF/ANSI 61 –2016, Drinking water system components – health effects, 2016.
- [29] Quasar: 10.5281/zenodo.1188775
- [30] F. Pedregosa, et al., Scikit-Learn: machine learning in python, *J. Mach. Learn. Res.* 12 (2011) 2825–2830.
- [31] D.L. Pavia, G.M. Lampman, G.S. Kriz, *Introduction to Spectroscopy*, 3rd ed., Thomson Learning, 2001.
- [32] J.W. Moore, R.G. Pearson, *Kinetics and Mechanism*, John Wiley & Sons, New York, 1981 p. 26.
- [33] I. Noda, Close-up view on the inner workings of two-dimensional correlation spectroscopy, *Vib. Spectrosc.* 60 (2012) 146–153.
- [34] Y. Park, I. Noda, Y.M. Jung, Two-dimensional correlation spectroscopy in polymer study, *Front. Chem.* 3 (2015) 14.
- [35] S. Morita, 2DPy Jupyter notebook accessed from <https://github.com/shigemorita/2Dpy> on July 18, 2021.
- [36] <https://polymer-additives.specialchem.com/product/a-basf-tinuvin-622-sf>, accessed November 28, 2021.
- [37] J.N. Hahladakis, C.A. Velis, R. Weber, E. Iacovidou, P. Purnell, An overview of chemical additives present in plastics: migration, release, fate and environmental impact during their use, disposal and recycling, *J. Hazard. Mater.* 344 (2018) 179–199.
- [38] J.V. Gulmine, L. Akcelrud, FTIR characterization of aged XLPE, *Polym. Test.* 25 (7) (2006) 932–942.
- [39] S.A. Jabarin, E.A. Lofgren, Photooxidative effects on properties and structure of high-density polyethylene, *J. Appl. Polym. Sci.* 53 (4) (1994) 411–423.
- [40] R. Satoto, W.S. Subowo, R. Yusiasih, Y. Takane, Y. Watanabe, T. Hatakeyama, Weathering of high-density polyethylene in different latitudes, *Polym. Degrad. Stab.* 56 (3) (1997) 275–279.
- [41] A. Fairbrother, H. Hsueh, J. Kim, D. Jacobs, L. Perry, D. Goodwin, C. White, S. Watson, L. Sung, Temperature and light intensity effects on photodegradation of high-density polyethylene, *Polym. Degrad. Stab.* 165 (2019) 153–160.
- [42] A.C. Albertsson, C. Barenstedt, S. Karlsson, Susceptibility of enhanced environmentally degradable polyethylene to thermal and photo-oxidation, *Polym. Degrad. Stab.* 37 (2) (1992) 163–171.
- [43] L. Küpper, J.V. Gulmine, P.R. Janissek, H.M. Heise, Attenuated total reflection infrared spectroscopy for micro-domain analysis of polyethylene samples after accelerated ageing within weathering chambers, *Vib. Spectrosc.* 34 (1) (2004) 63–72.
- [44] Y. Zhang, Z. Hou, K. Wu, S. Wang, J. Li, S. Li, Influence of oxygen diffusion on thermal ageing of cross-linked polyethylene cable insulation, *Materials* 13 (9) (2020) 2056.
- [45] M. Bertoldo, F. Ciardelli, Water extraction and degradation of a sterically hindered phenolic antioxidant in polypropylene films, *Polymer* 45 (26) (2004) 8751–8759.
- [46] S. Beißmann, M. Stiftinger, K. Grabmayer, G. Wallner, D. Nitsche, W. Buchberger, Monitoring the degradation of stabilization systems in polypropylene during accelerated aging tests by liquid chromatography combined with atmospheric pressure chemical ionization mass spectrometry, *Polym. Degrad. Stab.* 98 (9) (2013) 1655–1661.
- [47] K. Nagy, E. Epacher, P. Staniek, B. Pukánszky, Hydrolytic stability of phenolic antioxidants and its effect on their performance in high-density polyethylene, *Polym. Degrad. Stab.* 82 (2) (2003) 211–219.
- [48] D. Tátraaljai, M. Vámos, Á. Orbán-Mester, P. Staniek, E. Földes, B. Pukánszky, Performance of PE pipes under extractive conditions: effect of the additive package and processing, *Polym. Degrad. Stab.* 99 (2014) 196–203.
- [49] E. Reingruber, W. Buchberger, Analysis of polyolefin stabilizers and their degradation products, *J. Sep. Sci.* 33 (22) (2010) 3463–3475.
- [50] R.K. Rowe, F.B. Abdelaal, Antioxidant depletion in high-density polyethylene (HDPE) geomembrane with hindered amine light stabilizers (HALS) in low-pH heap leach environment, *Can. Geotech. J.* 53 (10) (2016) 1612–1627.
- [51] T.G. Solomons, C.B. Fryhle, *Organic Chemistry*, John Wiley & Sons, 2008.